The scattering of x rays from nonideal multilayer structures

D. G. Stearns

Lawrence Livermore National Laboratory, P. O. Box 808, Livermore, California 94550

A general theory is developed for the scattering of x rays from a single nonideal interface between two dielectric media. It is then extended to describe the scattering of x rays from a multilayer structure composed of many nonideal interfaces. The most unique feature of this theory is that there are no constraints on the physical structure of the interfaces; the interfaces can have any form of roughness or compositional inhomogeneity. A simple analytical expression is derived for both the near and far radiation field to first order, assuming that the scattering is weak. The theory is valid for arbitrary polarization and at all angles of incidence (measured from the normal) less than the critical angle for total external reflection. Finally, the results are applied to study the effect of different interface structures on the performance of multilayer x-ray optics.

I. INTRODUCTION

Recent progress in the controlled deposition of ultrathin multilayer structures has had a large impact in the field of x-ray optics.[1] A synthetically fabricated structure composed of many alternating layers of high-X and low-X materials can produce normal incidence reflectance of tens of percent at x-ray wavelengths, several orders of magnitude greater than the reflectance of a single surface (typically $\sim 10^{-4}$). This property has spurred the development of a new class of reflection optics for the soft x-ray wavelength region of ~ 1–30 nm. Comprehensive descriptions of the design, fabrication, and characterization of x-ray multilayer mirrors can be found elsewhere.[2-18] Indeed, x-ray multilayer optics are now used in many applications, including x-ray astronomy, microscopy, spectroscopy, as filters and monochromators for intense sources such as synchrotron radiation and in x-ray laser cavities.[19-28]

Designing optimized multilayer x-ray optics for specific applications requires the ability to accurately calculate the scattering of x rays from these structures. The simplest and most common method is to assume that the multilayer is composed of ideal layers. The reflectance and transmittance of a system of ideal interfaces can be determined from the Fresnel equations for the scattering from a single interface in conjunction with recursive[29] or matrix[30] methods to treat the multiple scattering within the layered structure. It is generally found, however, that calculations based on the simple model of ideal layers yield results that are in substantial disagreement with the measured performance. A major reason for the disparity is the failure of the simple model to account for realistic interfaces. In practice, the interfaces between materials that are not well lattice-matched are far from ideal on the spatial scale of an x-ray wavelength. Many of the material combinations preferred for x-ray multilayer optics, such as tungsten and carbon, exhibit significant polycrystalline growth and compound formation at the layer boundaries, resulting in rough and extended interface regions.[31-34] The nonideal interfaces not only modify the specular scattering, but can also scatter x rays into nonspecular directions.

Hence, the quantitative calculation of the scattering properties of a multilayer x-ray optical component requires both an accurate description of the interfaces and a comprehensive theory of the interaction of x rays with the nonideal structure.

The scattering of electromagnetic radiation from a nonideal interface has been an important problem in applied physics. Much of the early work[35] was directed towards understanding the behavior of radio waves (and radar) scattered from the surface of the earth. In particular, Beckmann and Spizzichino[36] (BS) developed a comprehensive scalar scattering theory that applies to a rough surface for which the radius of curvature is much greater than a wavelength of the radiation. Concurrently, there has been a substantial theoretical effort to describe the scattering of light from rough surfaces. The specular reflectance at normal incidence has been related to the distribution of surface heights, establishing light scattering as a diagnostic measurement of surface roughness.[37,38] There have been several treatments of the scattering of light from thin films[39,40] and multilayer mirrors[41,42] having rough interfaces, which are essentially extentions of the BS theory. More rigorous analytical[43,44] and numerical[45,46] methods have been presented for calculating the light scattered from "slightly rough" surfaces. The term "slightly rough" refers to the condition where the deviations of the surface from the ideal plane are much smaller than the wavelength of the light.

In the regime of shorter wavelengths an early effort was made to give a theoretical treatment of the scattering of x rays from a nonideal interface.[47] A numerical method has been developed by Nevot and Croce[48] for calculating the specular scattering of electromagnetic radiation near grazing incidence, and has been extended by Croce[49] for the more general case of a stratified medium. Vidal and Vincent[50] have applied an analytical technique based on reciprocity relations[51] to determine the specular reflectance and transmittance of x rays from a nonideal multilayer stack. Their result is limited to the special case where the layers are "slightly rough" in one dimension. More recently, Sinha *et al.*[52] have developed a scalar theory for the scattering of x

rays and neutrons from a rough surface that can be described statistically in terms of a Gaussian random variable.

It is evident that the complexity of the problem of the scattering of electromagnetic radiation from an arbitrary interface precludes an exact analytical solution. Unfortunately, all of the previous theories place restrictions on the scattering conditions and on the nature of the interfaces that can pose undesirable limitations when calculating the x-ray scattering from realistic interface structures. In particular, we identify three important requirements: (1) The scattering theory should be applicable to any type of interface structure including the important special cases of rough and compositionally inhomogeneous interfaces; (2) there should be no constraints on the spatial extent of the interface region; and (3) the theory should be valid for any configuration of the incident field.

The purpose of this paper is to develop a general scattering theory that satisfies these basic criteria. The scattering of x rays from an interface is weak except near grazing incidence, since all materials have dielectric constants near unity at x-ray wavelengths. This property is exploited in Sec. II to derive a first-order analytical solution for the total field scattered by a single interface of arbitrary structure. The theory is valid for all polarizations and at any angle of incidence away from grazing incidence.

In Sec. III the theory is extended to describe the scattering of x rays from a system of nonideal interfaces. A numerical method is presented for calculating the reflectance, transmittance, and the nonspecular scattering from a nonideal multilayer structure. The interaction of the interfaces is treated in the "specular field approximation," wherein the multiple scattering of the nonspecular field is neglected. As an application of the theory, we calculate the reflectance and transmittance of two representative multilayer x-ray beamsplitters, and investigate the effect of different interface structures on their performance.

II. THE SCATTERING OF X RAYS FROM A SINGLE NONIDEAL INTERFACE

A. Scattering theory formalism

We begin by deriving a general expression that describes the scattering of x rays from an arbitrary spatial inhomogeneity. The scattering from an interface between two dielectric media is then treated as a special configuration of the general scattering problem.

Consider the propagation of x rays in a medium represented by a dielectric function $\epsilon(x, \omega)$, which relates the displacement field D to the electric field E (assuming a harmonic time dependence $e^{i\omega t}$) through

$$D(x, \omega) = \epsilon(x, \omega) E(x, \omega). \tag{1}$$

The implications and limitations of the dielectric function representation of matter are discussed in Appendix A. At x-ray wavelengths, the dielectric function is typically a complex quantity, the imaginary part corresponding to the attenuation of the electromagnetic field in the medium. For simplicity of presentation, however, the dielectric function is assumed to be purely real throughout the derivations in Secs. II B and II C. The modification of the theory to accommo-

date a complex dielectric function is the subject of Sec. II D.

Let the incident field E^0 be defined as the field that propagates in a uniform medium of dielectric constant ϵ_0. In particular, the incident field is a solution of the homogeneous wave equation,

$$(\nabla^2 + k^2)E^0 = 0, \tag{2}$$

where $k^2 = \epsilon_0(\omega/c)^2$.

Now consider the introduction of a spatial inhomogeneity $\alpha(x)$ defined as the deviation of the dielectric function from its uniform value,

$$\alpha(x) = \epsilon(x) - \epsilon_0. \tag{3}$$

The incident field is scattered from the spatial inhomogeneity, producing a scattered field E^{sc} that satisfies the inhomogeneous differential equation,[53]

$$(\nabla^2 + k^2)D^{sc}(x) = -\nabla \times \nabla \times \alpha(x)[E^0(x) + E^{sc}(x)]. \tag{4}$$

At x-ray wavelengths, the dielectric constant for all materials is close to unity. Consequently, any variations in the dielectric function must be small so that $\alpha(x) \ll 1$. Inspection of (4) suggests that when α is small, the scattered field is weak. Hence, the scattered field is estimated to first order by neglecting E^{sc} on the right-hand side of (4) (the Born approximation).

An analytic solution for the scattered field is obtained through the method of Fourier transformation. The incident field is chosen to be a plane wave propagating in the direction $\hat{n}^0$ with polarization $\hat{e}^0$,

$$E^0(x) = \hat{e}^0 \exp(ik\hat{n}^0 \cdot x). \tag{5}$$

Using the usual relationship between a function $f(x)$ and its Fourier transform $\tilde{f}(s)$, we take the Fourier transform of both sides of Eq. (4) to find

$$\tilde{D}^{sc}(s) = [(\hat{n} \times \hat{e}^0) \times \hat{n}][s^2/(s^2 - k^2)]\tilde{\alpha}(s - k\hat{n}^0), \tag{6}$$

where $s \equiv s\hat{n}$. An expression for the scattered field is obtained through the inverse Fourier transform of (6),

$$D^{sc}(x) = \frac{1}{(2\pi)^3} \int [(\hat{n} \times \hat{e}^0) \times \hat{n}]$$
$$\times \tilde{\alpha}(s - k\hat{n}^0)\frac{s^2}{s^2 - k^2} e^{is \cdot x} ds. \tag{7}$$

Next we specialize the result to the case of the scattering of x rays by an interface. In particular, we choose the variation α to represent a second uniform medium of dielectric constant ϵ_0' located in the half space $z < 0$ such that

$$\alpha(x) = \begin{cases} 0 & z \to +\infty \\ \Delta & z \to -\infty \end{cases}, \tag{8}$$

where $\Delta \equiv \epsilon_0 - \epsilon_0'$. As shown schematically in Fig. 1, the interface corresponds to the region of transition between the two media in the vicinity of the plane $z = 0$.

The interface can be described formally by a function $g(x)$ defined as the normalized derivative of $\alpha(x)$ along the z direction,

$$g(x) \equiv \frac{1}{\Delta}\frac{\partial \alpha(x)}{\partial z} = \frac{1}{\Delta}\frac{\partial \epsilon(x)}{\partial z}. \tag{9}$$

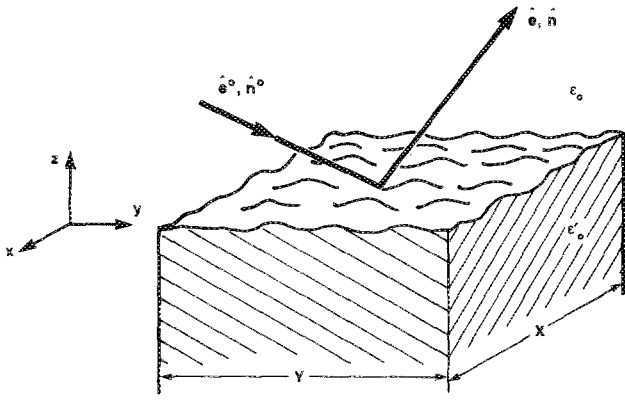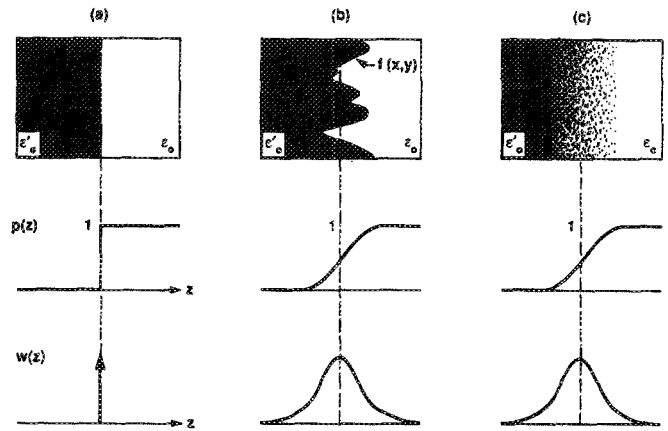FIG. 1. Configuration of the x-ray scattering from a single interface.

FIG. 2. One-dimensional representations of different types of interfaces having profiles $p(z)$ and derivatives $w(z)$. (a) An ideal interface; (b) a purely rough interface; and (c) a purely diffuse interface.

In addition, we define the origin of the z axis by requiring that

$$\int z g(\mathbf{x}) d\mathbf{x} = 0. \tag{10}$$

In order to keep the scattered power finite, the lateral area of the interface is considered to be bounded, extending for a rectangular region $-X/2 < x < X/2$ and $-Y/2 < y < Y/2$. Then the interface encompasses an area in the x-y plane equal to

$$XY = \int g(\mathbf{x}) d\mathbf{x} = \tilde{g}(0). \tag{11}$$

In the remainder of this paper, the limit $X, Y \to \infty$ is implicitly assumed to avoid diffraction from the edges of the interface.

The specular components of the scattered field are only sensitive to the average variation of the dielectric function across the interface. Consequently, it is useful to introduce the interface profile function $p(z)$, defined as the normalized average value of the dielectric function along the z direction,

$$p(z) \equiv \frac{1}{\Delta} \frac{\int\int \left[\epsilon(\mathbf{x}) - \epsilon_0' \right] dx \, dy}{\int\int dx \, dy}$$

$$= \frac{1}{\Delta \tilde{g}(0)} \int\int \left[\epsilon(\mathbf{x}) - \epsilon_0' \right] dx \, dy. \tag{12}$$

We also define $w(z)$ as the derivative of the interface profile,

$$w(z) = \frac{dp(z)}{dz}. \tag{13}$$

The advantage of this formalism is its complete generality; the functions $g(\mathbf{x})$, $p(z)$, and $w(z)$ can represent an interface of arbitrary structure. To illustrate the role of these functions, three special types of interfaces are presented in Fig. 2. The ideal interface is shown in Fig. 2(a), in which the transition between two media having dielectric constants ϵ_0 and ϵ_0' occurs abruptly at $z = 0$. The profile $p(z)$ is a unit step function and the interface is characterized by the delta function $g(\mathbf{x}) = w(z) = \delta(z)$. A purely rough interface is shown in Fig. 2(b). In this case the interface profile $p(z)$ is smooth even though the transition between the media at any position (x,y) is abrupt. In particular, the boundary between the two media can be defined by a surface $z = f(x,y)$. Since the dielectric function is discontinuous at the surface, then

$g(\mathbf{x}) = \delta[z - f(x,y)]$ and $w(z)$ represents the normalized distribution of surface heights $f(x,y)$ about the plane $z = 0$. In contrast, Fig. 2(c) shows a purely diffuse interface, in which the dielectric constant varies smoothly along the z direction and is uniform in the x-y plane. In this case $p(z)$ represents the actual variation of composition across the interface and $g(\mathbf{x}) = g(z) = w(z)$ is the composition gradient.

B. The reflected field

The configuration of the scattering problem is depicted in Fig. 1. An incident plane wave propagates from medium ϵ_0 to medium ϵ_0' in a direction $\hat{n}^0$ with initial polarization $\hat{e}^0$, and scatters into a direction $\hat{n}$ with polarization $\hat{e}$. The reflected and transmitted fields correspond to scattering in which $n_z > 0$ and $n_z < 0$, respectively. We consider first the derivation of the reflected field $\mathbf{E}^r$.

The Fourier transform of $g(\mathbf{x})$ is given by

$$\tilde{g}(\mathbf{s}) = (i s_z / \Delta) \tilde{\alpha}(\mathbf{s}). \tag{14}$$

Substitution for $\tilde{\alpha}$ in (7) yields an expression for the reflected field in the Born approximation,

$$\mathbf{E}^r(\mathbf{x}) = \frac{-i\Delta}{(2\pi)^3 \epsilon_0} \int \left[(\hat{n} \times \hat{e}^0) \times \hat{n} \right]$$

$$\times \tilde{g}(\mathbf{s} - k\hat{n}^0) \frac{s^2 e^{i\mathbf{s}\cdot\mathbf{x}} \, d\mathbf{s}}{(s_z - k n_z^0)(s^2 - k^2)}. \tag{15}$$

Defining g^* as the partial Fourier transform of g such that

$$\int g^*(s_x, s_y, z') e^{-i s_z z'} \, dz' = \tilde{g}(\mathbf{s}), \tag{16}$$

we can separate the integration over s_z in (15) to obtain

$$\mathbf{E}^r(\mathbf{x}) = \frac{-i\Delta}{(2\pi)^3 \epsilon_0} \int\int\int \left(\int s^2 [(\hat{n} \times \hat{e}^0) \times \hat{n}] \right.$$

$$\times \frac{e^{i s_z (z - z')} \, ds_z}{(s_z - k n_z^0)(s_z + \xi)(s_z - \xi)} \right)$$

$$\times g^*(s_x - k n_x^0, s_y - k n_y^0, z')$$

$$\times e^{i s_x x} e^{i s_y y} e^{i k n_z^0 z'} \, ds_x \, ds_y \, dz', \tag{17}$$

where

$$\xi \equiv \sqrt{k^2 - s_x^2 - s_y^2}. \qquad (18)$$

The integral over s_z in (17) is evaluated using contour integration. The scattered field must be evaluated at a position $\mathbf{x}$ that is completely outside of the interface region. Specifically, it is required that $z > z'$ for all points $\mathbf{x}'$ at which $g(\mathbf{x}')$ is nonzero. Then the factor $\exp[is_z(z - z')]$ allows the contour to be closed with a semicircle of infinite radius lying in the upper s_z plane. The integrand has poles at $s_z = kn_z^0, \pm \xi$. The poles are actually displaced above and below the real axis, because the causality of $\mathbf{E}^r$ requires that the frequency ω must have a small positive imaginary part[54] making the wave number k imaginary. Only the pole at $s_z = +\xi$ is enclosed by the contour and contributes to the integral (recall that $n_z^0 < 0$). Evaluation of the residue of the integrand requires from (19) that $s = k$ and $n_z = (1 - n_x^2 - n_y^2)^{1/2}$. Then, the integration yields

$$\mathbf{E}^r(\mathbf{x}) = \frac{\Delta k^2}{8\pi^2 \epsilon_0} \int\int [(\hat{n} \times \hat{e}^0) \times \hat{n}]$$

$$\times \frac{\tilde{g}(k\hat{n} - k\hat{n}^0)}{n_z(n_z - n_z^0)} e^{ik\hat{n}\cdot\mathbf{x}} \, dn_x \, dn_y. \qquad (19)$$

The component of the scattered field having polarization $\hat{e}$ can be written as

$$\hat{e}^* \cdot \mathbf{E}^r(\mathbf{x}) = \int\int r(\hat{n}, \hat{e}; \hat{n}^0, \hat{e}^0) e^{ik\hat{n}\cdot\mathbf{x}} \, dn_x \, dn_y, \qquad (20)$$

where $\hat{e}^*$ is the complex conjugate of the polarization vector (required for circular polarization) and the mode amplitude density $r(\hat{n}, \hat{e}; \hat{n}^0, \hat{e}^0)$ is defined by

$$r(\hat{n}, \hat{e}; \hat{n}^0, \hat{e}^0) = \frac{\Delta k^2}{8\pi^2 \epsilon_0} (\hat{e}^* \cdot \hat{e}^0) \frac{\tilde{g}(k\hat{n} - k\hat{n}^0)}{n_z(n_z - n_z^0)}. \qquad (21)$$

It is evident in (20) that the reflected field is a superposition of plane wave modes and evanescent modes. As usual, the evanescent modes correspond to fields that decrease exponentially with distance from the interface. They are associated with imaginary values of n_z, which occurs when $n_x^2 + n_y^2 > 1$.

The scattered radiation in the far-field is derived by letting $\mathbf{x} = R\hat{n}$ in the limit as $R \to \infty$. As the point of observation is removed far from the interface,[55] the field is dominated by the mode that propagates in the direction $\hat{n}$. It is shown in Appendix B that the scattered field becomes

$$\hat{e}^* \cdot \mathbf{E}^r(\mathbf{x} = R\hat{n}) \overset{R\to\infty}{=} -\frac{2\pi i n_z}{k} r(\hat{n}, \hat{e}; \hat{n}^0, \hat{e}^0) \frac{e^{ikR}}{R}. \qquad (22)$$

Introducing the momentum transfer vector $\mathbf{q} \equiv k\hat{n} - k\hat{n}^0$, Eq. (22) can be rewritten as

$$\hat{e} \cdot \mathbf{E}^r(\mathbf{q}) = -\frac{i\Delta k^2}{4\pi\epsilon_0 q_z} (\hat{e}^* \cdot \hat{e}^0)\tilde{g}(\mathbf{q}) \frac{e^{ikR}}{R}. \qquad (23)$$

It is evident that the x rays scattered from the interface with a change of momentum $\mathbf{q}$ are described in the far field by an outgoing spherical wave with an amplitude proportional to $\tilde{g}(\mathbf{q})$. Physically, $\tilde{g}(\mathbf{q})$ represents the frequency spectrum of the spatial inhomogeneities that compose the interface region. It is also interesting to observe that the solution is consistent with the principal of reciprocity, as the amplitude of the scattered field is unchanged under the transformation

$\hat{n} \Leftrightarrow -\hat{n}^0$. The analytical expression (23) can be compared to the results of Croce[49] for the special case of a stratified interfacial region to obtain a useful geometrical interpretation of the scattering process.

The quantity most relevant to experiment is the scattered power. The differential power dP^r scattered into solid angle $d\Omega$ with propagation vector $\hat{n}$ and polarization $\hat{e}$ per unit incident power having propagation vector $\hat{n}^0$ and polarization $\hat{e}^0$ is given by

$$\frac{dP^r}{d\Omega}(\hat{n}, \hat{e}; \hat{n}^0, \hat{e}^0) = \frac{4\pi^2 |n_z^0|}{k^2 \tilde{g}(0)} |r(\hat{n}, \hat{e}; \hat{n}^0, \hat{e}^0)|^2$$

$$= \frac{1}{16\pi^2 |n_z^0|} \left| \frac{\Delta k^2}{\epsilon_0 q_z} (\hat{e}^* \cdot \hat{e}^0) \right|^2 \frac{|\tilde{g}(\mathbf{q})|^2}{\tilde{g}(0)}. \qquad (24)$$

Except for the geometrical and polarization factors, the angular distribution of the scattered power is simply related to the structure of the interface through the term $|\tilde{g}(\mathbf{q})|^2$.

C. The transmitted field

The derivation of the radiation field transmitted through a nonideal interface follows closely the case of the reflected field. We begin by modifying Eq. (7), replacing the wave number k with k'. The motivation for this procedure is best understood by studying Eq. (4). The left-hand side is the wave equation, describing the propagation of waves in the medium ϵ_0, and the right-hand side is the source term. The transmitted field, however, is necessarily composed of waves propagating in the medium ϵ_0'. Replacing k with k' in the wave equation resolves this inconsistency. Then, the transmitted field $\mathbf{E}^t$ is given by

$$\mathbf{E}^t(\mathbf{x}) = \frac{-i\Delta}{(2\pi)^3 \epsilon_0'} \int [(\hat{n} \times \hat{e}^0) \times \hat{n}]$$

$$\times \tilde{g}(\mathbf{s} - k\hat{n}^0) \frac{s^2 e^{i\mathbf{s}\cdot\mathbf{x}} \, d\mathbf{s}}{(s_z - kn_z^0)(s^2 - k'^2)}, \qquad (25)$$

which is rewritten as

$$\mathbf{E}^t(\mathbf{x}) = \frac{-i\Delta}{(2\pi)^3 \epsilon_0'} \int\int\int \left(\int s^2 [(\hat{n} \times \hat{e}^0) \times \hat{n}] \right.$$

$$\times \frac{e^{is_z(z-z')} \, ds_z}{(s_z - kn_z^0)(s_z + \xi')(s_z - \xi')} \Bigg)$$

$$\times g(s_x - kn_x^0, s_y - kn_y^0, z')$$

$$\times e^{is_x x} e^{is_y y} e^{ikn_z^0 z'} \, ds_x \, ds_y \, dz', \qquad (26)$$

where

$$\xi' \equiv \sqrt{k'^2 - s_x^2 - s_y^2}. \qquad (27)$$

As before, the integral over s_z is evaluated by contour integration. In this case, however, the field is evaluated at a point $\mathbf{x}$ outside of the interface region such that $z < z'$ for all points $\mathbf{x}'$ for which $g(\mathbf{x}')$ is nonzero. The exponential factor allows the contour to be closed with a semicircle of infinite radius in the lower s_z plane. The two poles at $s_z = kn_z^0, -\xi'$ are enclosed by the contour and contribute to the integral. Evaluation of the residues of the integrand at these poles yields two

terms E_1' and E_2'. It is easily shown that the contribution from the pole at $s_z = k n_z^0$ is given by

$$E_1'(\mathbf{x}) = -\hat{e}_0 e^{ik\hat{n}^0 \cdot \mathbf{x}}$$

$$= -E^0(\mathbf{x}). \tag{28}$$

Hence, this part of the scattered field exactly cancels the incident field in medium ϵ_0'. The remaining transmitted field corresponds to the contribution from the pole at $z = -\xi'$. Evaluation of (27) at this pole requires that $s = k'$ and $n_z = (1 - n_x^2 - n_y^2)^{1/2}$. The residue yields

$$E_2'(\mathbf{x}) = E'(\mathbf{x}) = -\frac{\Delta k'^3}{8\pi^2 \epsilon_0'} \int\int [(\hat{n} \times \hat{e}^0) \times \hat{n}]$$

$$\times \frac{\tilde{g}(k'n - k\hat{n}^0)}{n_z(k'n_z - kn_z^0)} e^{ik'\hat{n} \cdot \mathbf{x}} \, dn_x \, dn_y. \tag{29}$$

The transmitted field can be expressed in terms of a mode amplitude density $t(\hat{n}, \hat{e}; \hat{n}^0, \hat{e}^0)$,

$$\hat{e}^* \cdot E'(\mathbf{x}) = \int t(\hat{n}, \hat{e}; \hat{n}^0, \hat{e}^0) e^{ik'\hat{n} \cdot \mathbf{x}} \, dn_x dn_y, \tag{30}$$

where

$$t(\hat{n}, \hat{e}; \hat{n}^0, \hat{e}^0) = -\frac{\Delta k'^3}{8\pi^2 \epsilon_0'} (\hat{e}^* \cdot \hat{e}^0) \frac{\tilde{g}(k'n - k\hat{n}^0)}{n_z(k'n_z - kn_z^0)}. \tag{31}$$

We observe that the transmitted field is a superposition of plane waves, including the properly refracted incident field, propagating in the medium ϵ_0'.

An expression for the transmitted radiation in the far field is derived following the procedure outlined in Appendix B with the result

$$\hat{e}^* \cdot E'(\mathbf{q}) = -\frac{i\Delta k'^2}{4\pi\epsilon_0' q_z} (\hat{e}^* \cdot \hat{e}^0) \tilde{g}(\mathbf{q}) \frac{e^{ik'R}}{R}, \tag{32}$$

where the momentum transfer vector is now defined as $\mathbf{q} = k'\hat{n} - k\hat{n}_0$. Similarly, the transmitted power scattered per unit solid angle is given by

$$\frac{dP'}{d\Omega}(\hat{n}, \hat{e}; \hat{n}^0, \hat{e}^0) = \frac{4\pi^2 |n_z^0|}{k'^2 \tilde{g}(0)} |t(\hat{n}, \hat{e}; \hat{n}^0, \hat{e}^0)|^2$$

$$= \frac{1}{16\pi^2 |n_z^0|} \left| \frac{\Delta k'^2}{\epsilon_0' q_z} (\hat{e}^* \cdot \hat{e}^0) \right|^2 \frac{|\tilde{g}(\mathbf{q})|^2}{\tilde{g}(0)}. \tag{33}$$

A comparison of (33) and (24) shows that, for a given momentum transfer $\mathbf{q}$, the power scattered by the interface into the reflected and transmitted fields is identical to second order in Δ.

D. Absorbing media

Thus far we have assumed that the dielectric function is purely real. In fact, the absorption of soft x rays in the wavelength range of 1–30 nm is significant for most materials. Consequently, it is important to treat the dielectric function as a complex quantity, the imaginary part accounting for the attenuation of the radiation field in the medium.

The results of the previous sections can be directly modified to accommodate a complex dielectric function. In particular, since the amplitude of the incident and scattered fields must be finite over the entire interface, they can attenuate only in the z direction, requiring that n_x and n_y be real, as well as the wave numbers $k = |\epsilon_0^{1/2}| k_0$ and $k' = |\epsilon_0'^{1/2}| k_0$. Thus, only n_z is complex and is given by

$$n_z = \begin{cases} \sqrt{\dfrac{\epsilon_0}{|\epsilon_0|} - n_x^2 - n_y^2} & \text{reflected field} \\[4mm] \sqrt{\dfrac{\epsilon_0'}{|\epsilon_0'|} - n_x^2 - n_y^2} & \text{transmitted field.} \end{cases} \tag{34}$$

The plane waves $\exp(ik\hat{n} \cdot \mathbf{x})$ and $\exp(ik'\hat{n} \cdot \mathbf{x})$ that compose the scattered fields now exhibit the curious property of propagating and attenuating in different directions. The imaginary part of n_z is chosen to be positive for the reflected field and negative for the transmitted field to ensure that the scattered field decays exponentially away from the interface. It is also assumed that the decay of the radiation field across the interface is negligible. Then, n_z can be replaced by its real part for any integrations over the interface region, such as in the Fourier transformation of $g(\mathbf{x})$.

With these modifications, expressions (20) and (30) remain valid descriptions of the reflected and transmitted fields, respectively. The mode amplitude densities become

$$r(\hat{n}, \hat{e}; \hat{n}^0, \hat{e}^0) = \frac{\Delta k^2}{8\pi^2 |\epsilon_0|} (\hat{e}^* \cdot \hat{e}^0) \frac{\tilde{g}[\text{Re}(k\hat{n} - k\hat{n}^0)]}{n_z(n_z - n_z^0)},$$

$$t(\hat{n}, \hat{e}; \hat{n}^0, \hat{e}^0) = -\frac{\Delta k'^3}{8\pi^2 |\epsilon_0'|} (\hat{e}^* \cdot \hat{e}^0) \frac{\tilde{g}[\text{Re}(k'\hat{n} - k\hat{n}^0)]}{n_z(k'n_z - kn_z^0)}. \tag{35}$$

An important consequence of a complex dielectric function is that the poles in the contour integrals (17) and (26) are automatically moved off of the real axis. The position of the pole is determined from the sign of the imaginary part of n_z. Hence, the causality of the solution is established by satisfying the physical constraint that the scattered fields must attenuate away from the interface.

E. Discussion

The expressions derived above provide a general description of the radiation field scattered by a nonideal interface of arbitrary structure, restricted only by the requirement that the scattering is weak so that the first-order Born approximation of the scattered field is appropriate. Despite some mathematical complexity, the analytical solutions provide valuable insight into the nature of the scattered field. The mode structure of the field is directly related to the physical structure of the interface through the function $\tilde{g}(\mathbf{q})$. Inspection of Eqs. (24) and (33) shows that the distribution of energy among the propagating modes is proportional to $|\tilde{g}(\mathbf{q})|^2$, which corresponds to the power spectrum of the spatial variations of the dielectric function at the interface. We now consider several special cases of practical importance to illustrate the physical relationship between the structure of the interface and the scattered field.

1. The ideal interface

The ideal interface corresponds to an abrupt transition between two media at the plane $z = 0$, and represents the simplest possible configuration of an interface. Since the exact solution of the scattering from an ideal interface is well known, it also serves as a valuable test of the first-order scattering theory.

The ideal interface is represented by the delta function $g(\mathbf{x}) = \delta(z)$. Taking the Fourier transform, and substituting into (23) for the reflected field yields

$$\hat{e}^* \cdot \mathbf{E}^r(\mathbf{x}) = \frac{\Delta}{4|\epsilon_0|n_z^{0^2}} (\hat{e}^* \cdot \hat{e}^0) e^{ik\hat{n}^r \cdot \mathbf{x}}, \tag{36}$$

where

$$n_x^r = n_x^0, \quad n_y^r = n_y^0, \quad n_z^r = -n_z^0. \tag{37}$$

Hence, we derive a well-known result: The field reflected from an ideal interface is composed of a single plane wave propagating in the specular direction $\hat{n}^r$. Using (32), we obtain an expression for the transmitted field to first order in Δ,

$$\hat{e}^* \cdot \mathbf{E}^t(\mathbf{x}) = \left(1 + \frac{\Delta}{4|\epsilon_0|n_z^{0^2}}\right)(\hat{e}^* \cdot \hat{e}^0) e^{ik'\hat{n}^t \cdot \mathbf{x}}, \tag{38}$$

where $\hat{n}^t$ is the direction of specular transmission given by

$$n_x^t = \frac{k}{k'} n_x^0, \quad n_y^t = \frac{k}{k'} n_y^0,$$

$$n_z^t = \sqrt{\frac{\epsilon_0'}{|\epsilon_0'|} - \left(\frac{k}{k'} n_x^0\right)^2 - \left(\frac{k}{k'} n_y^0\right)^2}. \tag{39}$$

It can be shown that the exact solution for the field scattered from an ideal interface, as given by the Fresnel equations, agrees with (36) and (38) in the limit

$$\Delta/n_z^{0^2} \ll 1. \tag{40}$$

This condition formally represents the requirement of weak scattering upon which the first-order scattering theory is based. The scattering is weak when $\Delta = \epsilon_0 - \epsilon_0'$ is small (which is always true at x-ray wavelengths) *and* when n_z^0 is not near zero, that is, away from grazing incidence.

The constraint on n_z^0 is directly related to the condition for the total external reflection of x rays from an interface. In particular, consider the reflectance from an ideal interface between a material and vacuum. The real part of the index of refraction at x-ray wavelengths is typically written as $1 - \delta$, where δ is a small quantity. Then it can be shown[56] that the critical angle for total external reflection (measured from the surface) is given by $\theta_c \simeq (2\delta)^{1/2}$. Neglecting absorption, the dielectric constant of the material is $\epsilon = (1 - \delta)^2 \simeq 1 - 2\delta$. If θ_g is defined as the grazing angle of incidence of the x rays, measured from the plane $z = 0$, then for small grazing angles we have $n_z^0 = \theta_g$, and the condition (40) becomes $\theta_g \gg \theta_c$. Simply stated, the first-order scattering theory is valid providing the grazing angle of incidence is greater than the critical angle for total external reflection.

2. Specular scattering from a nonideal interface

We now consider the scattering of x rays from a nonideal interface. It is customary to divide the scattered field into specular and nonspecular components. By definition, the specular field conserves momentum in the x-y plane such that $q_x = q_y = 0$. Hence the specular field corresponds to scattering in the two directions $\hat{n}^r$ and $\hat{n}^t$ given by (37) and (39). Scattering into all other directions is nonspecular.

The calculation of the specular field requires the evaluation of $\tilde{g}(\mathbf{q})$ at $q_x = q_y = 0$. A simple manipulation yields

$$\tilde{g}(q_x = 0, q_y = 0, q_z) = \tilde{g}(0) \int w(z) e^{-iq_z z} \, dz = \tilde{g}(0)\tilde{w}(q_z). \tag{41}$$

This expression exhibits a unique characteristic of the specular field: Its amplitude depends only on the average variation of the dielectric function along the z direction. In particular, the specular scattering is completely determined from a knowledge of the derivative of the interface profile $w(z)$.

Substituting (42) into Eqs. (23) and (32), we arrive at general expressions for the amplitude densities $r(\hat{n}^r, \hat{e}; \hat{n}^0, \hat{e}^0)$ and $t(\hat{n}^t, \hat{e}; \hat{n}^0, \hat{e}^0)$ of the specular modes

$$r(\hat{n}^r, \hat{e}; \hat{n}^0, \hat{e}^0) = r^0 \tilde{w}[\operatorname{Re}(-2kn_z^0)],$$

$$t(\hat{n}^t, \hat{e}; \hat{n}^0, \hat{e}^0) = t^0 \tilde{w}[\operatorname{Re}(k'n_z^t - kn_z^0)]$$

$$\simeq t^0 \tilde{w}\{\operatorname{Re}[-(\Delta k/2|\epsilon_0|n_z^0)]\}, \tag{42}$$

where r^0 and t^0 are the Fresnel scattering amplitudes from an ideal interface. In the case of specular transmission, $\tilde{w}$ can be expanded in orders of Δ to obtain

$$\tilde{w}\left(-\frac{\Delta k}{2|\epsilon|n_z^0}\right) \simeq 1 - \left(\frac{\Delta k}{2|\epsilon|n_z^0}\right)^2 \int z^2 w(z) dz, \tag{43}$$

where the first-order term vanishes on account of (10). It is evident that the lowest-order correction of the specular transmission amplitude is second order in Δ. Hence, to first order the transmission through a nonideal interface is the same as through an ideal interface,
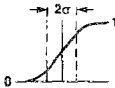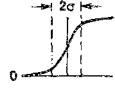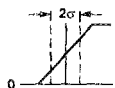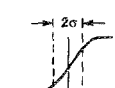
$$t(\hat{n}^t, \hat{e}; \hat{n}^0, \hat{e}^0) = t^0. \tag{44}$$

The evaluation of the specular scattering from a nonideal interface requires the determination of the profile function $p(z)$ and its derivative $w(z)$. Ideally, if the exact three-dimensional structure of the interface were known, then the actual profile $p(z)$ could be calculated numerically by averaging the dielectric function over the x and y directions. In general, however, such detailed knowledge of the structure of the interface is unavailable and it is more expedient to model the interface profile using a simple analytical function. It is convenient (but not necessary) to assume that $w(z)$ is a symmetric function. The width of the interface σ is defined by the second moment of $w(z)$,

$$\sigma^2 = \int z^2 w(z) dz. \tag{45}$$

Several useful models of the interface profile $p(z)$ are listed in Table I along with $w(z)$ and its Fourier transform $\tilde{w}(s)$. The appropriate choice of model is dictated largely by the nature of the interface. For instance, the classical diffusion of two materials produces a variation in composition at the interface described by an error function. When the interface profile $p(z)$ is modeled as an error function then $w(z)$ is a Gaussian. In contrast, the mixing at an interface produced by bombardment of the surface by energetic atoms during

496   J. Appl. Phys., Vol. 65, No. 2, 15 January 1989

D. G. Stearns   496

TABLE I. Several useful profiles $p(z)$ and the related functions $w(z)$ and $\tilde{w}(s)$.

Description of interface	$p(z)$	$w(z)$	$\tilde{w}(s)$
Error function	$\dfrac{1}{\sqrt{\pi}}\displaystyle\int_{-\infty}^{z} e^{-t^2/2\sigma^2}\,dt$	$\dfrac{1}{\sqrt{2\pi\sigma^2}}\,e^{-z^2/2\sigma^2}$	$e^{-\sigma^2 s^2/2}$
Exponential	$\begin{cases}\frac{1}{2}e^{\sqrt{2}z/\sigma}, & z\leqslant 0 \\ 1-\frac{1}{2}e^{-\sqrt{2}z/\sigma}, & z>0\end{cases}$	$\dfrac{1}{\sqrt{2\sigma^2}}\,e^{-\frac{\sqrt{2}|z|}{\sigma}}$	$\dfrac{1}{(1+s^2\sigma^2/2)}$
Linear	$\begin{cases}0, & z<-\sqrt{3}\sigma \\ \frac{1}{2}+\frac{z}{2\sqrt{3}\sigma}, & |z|\leqslant\sqrt{3}\sigma \\ 1, & z>\sqrt{3}\sigma\end{cases}$	$\begin{cases}0, & |z|>\sqrt{3}\sigma \\ \frac{1}{2\sqrt{3}\sigma}, & |z|\leqslant\sqrt{3}\sigma\end{cases}$	$\dfrac{\sin(\sqrt{3}\sigma s)}{\sqrt{3}\sigma s}$
Sinusoidal	$\begin{cases}0, & z<-a\sigma \\ \frac{1}{2}+\frac{1}{2}\sin\left(\frac{\pi z}{2a\sigma}\right), & |z|\leqslant a\sigma \\ 1, & z>a\sigma\end{cases}$ $a=\pi/\sqrt{\pi^2-8}$	$\begin{cases}0, & |z|>a\sigma \\ \frac{\pi}{4a\sigma}\cos\left(\frac{\pi z}{2a\sigma}\right), & |z|\leqslant a\sigma\end{cases}$	$\dfrac{\pi}{4}\left(\dfrac{\sin(a\sigma s-\pi/2)}{a\sigma s-\pi/2}+\dfrac{\sin(a\sigma s+\pi/2)}{a\sigma s+\pi/2}\right)$

sputter deposition might be better described by a linear compositional variation, and consequently $w(z)$ is the rectangle function. In the case of a rough interface, it has been suggested that the distribution of surface heights about the mean position, which is equivalent to $w(z)$, is best described by an exponential function.[57]

As a specific example, consider an interface of width σ having a profile represented by the error function

$$p(z) = \frac{1}{\sqrt{\pi}} \int_{-\infty}^{z} e^{-t^2/2\sigma^2}\,dt. \qquad (46)$$

Then the derivative $w(z)$ is the Gaussian,

$$w(z) = \frac{1}{\sqrt{2\pi\sigma^2}}\,e^{-z^2/2\sigma^2}, \qquad (47)$$

with a Fourier transform given by

$$\tilde{w}(s) = e^{-\sigma^2 s^2/2}. \qquad (48)$$

Substitution into (42) yields the well-known result

$$r(\hat{n}^r,\hat{e};\hat{n}^0,\hat{e}^0) = r^0 \exp(-2k^2 n_z^{0^2}\sigma^2), \qquad (49)$$

where the real part of n_z^0 is implied. It is seen that the amplitude density of specular reflection from an interface having an error function profile decreases exponentially with the unitless parameter $(\sigma/\lambda)^2$. If the width σ is much less than an x-ray wavelength, then the interface reflects essentially as if it were ideal. However, if the width is much greater than a wavelength, then the specular reflection amplitude is significantly attenuated. Inspection of the various forms for the

function $\tilde{w}(s)$ in Table I shows that this behavior is in fact common to all of the interface models.

3. Nonspecular scattering from a "slightly rough" interface

The scattering of radiation from a "slightly rough" interface is a case in which there is a conceptually simple relationship between the structure of the interface and the scattered field. This is also a problem of practical interest as it directly relates to the scattering from patterned surfaces such as gratings.

In general, a rough interface can be described by

$$g(\mathbf{x}) = \delta[z - f(x,y)], \qquad (50)$$

where the surface $f(x,y)$ defines the abrupt boundary between the two media. Taking the Fourier transform yields

$$\tilde{g}(\mathbf{q}) = \int\!\!\int e^{-iq_x x} e^{-iq_y y} e^{-iq_z f(x,y)}\,dx\,dy. \qquad (51)$$

The condition of "slight roughness" implies that the excursions of the surface $f(x,y)$ from the plane $z=0$ are small. In particular, it is required that $q_z f(x,y) \ll 1$ for all x, y. Then, the exponential is expanded to obtain

$$\tilde{g}(\mathbf{q}) \simeq (2\pi)^2 \delta(q_x)\delta(q_y) - iq_z\tilde{f}(q_x,q_y)$$

$$-\frac{q_z^2}{2}\int\!\!\int e^{-iq_x x} e^{-iq_y y}[f(x,y)]^2\,dx\,dy. \qquad (52)$$

The quantity of practical interest is the power scattered

by the interface. To derive the scattered power it is necessary to evaluate $|\tilde{g}|^2$. Squaring (52) yields

$$|\tilde{g}(\mathbf{q})|^2 = (2\pi)^2 \tilde{g}(0)\delta(q_x)\delta(q_y)(1 - q_z^2\sigma^2)$$
$$+ q_z^2|\tilde{f}(q_x,q_y)|^2, \tag{53}$$

where the cross term vanishes due to (10), and

$$\sigma^2 \equiv \frac{1}{\tilde{g}(0)} \int\int [f(x,y)]^2 \, dx \, dy. \tag{54}$$

The first and second terms correspond to the specular and nonspecular scattering, respectively. Ignoring specular reflection, we substitute the second term into (24) to find the differential power scattered per unit solid angle into the reflected field,

$$\frac{dP^r}{d\Omega}(\hat{n},\hat{e};\hat{n}^0,\hat{e}^0) = \frac{k^4}{16\pi^2|n_z^0|} \left| \frac{\Delta}{\epsilon_0}(\hat{e}^*\cdot\hat{e}^0) \right|^2$$
$$\times \frac{|\tilde{f}(q_x,q_y)|^2}{\tilde{g}(0)}. \tag{55}$$

It is straightforward to obtain a similar expression for the transmitted power. We observe that the scattering from a slightly rough surface exhibits remarkably simple behavior. In particular, the power distribution among the nonspecular modes is directly proportional to the power spectrum $|\tilde{f}(q_x,q_y)|^2$ of the surface roughness.

As an example, consider the field reflected from a sinusoidal grating described by

$$f(x,y) = a\cos(px) \tag{56}$$

having the Fourier transform

$$\tilde{f}(q_x,q_y) = (a/2)(2\pi)^2\delta(q_y)[\delta(q_x + p) + \delta(q_x - p)]. \tag{57}$$

Then, from (55) the power scattered per unit solid angle is

$$\frac{dP}{d\Omega}(\mathbf{q}) = \frac{a^2 k^4}{8|n_z^0|} \left| \frac{\Delta}{\epsilon_0}(\hat{e}^*\cdot\hat{e}^0) \right|^2$$
$$\times \delta(q_y)[\delta(q_x + p) + \delta(q_x - p)]. \tag{58}$$

The integration over solid angle is performed by using the relation $dq_x \, dq_y = k^2|n_z|d\Omega$. The result shows that power is scattered into only two nonspecular directions $\hat{n}^{\pm}$ given by

$$n_x^{\pm} = n_x^0 \pm p/k, \quad n_y^{\pm} = n_y^0, \quad n_z^{\pm} = \sqrt{1 - (n_x^0 \pm p)^2}. \tag{59}$$

The total power scattered in these directions is

$$P(\hat{n}^{\pm}) = 2a^2 k^2 \frac{|n_z^{0}|}{n_z^{\pm}} |r^0(0)|^2|\hat{e}^*\cdot\hat{e}^0|^2, \tag{60}$$

where $|r^0(0)|^2$ is the specular reflectivity of an ideal interface at normal incidence. Hence, the scattering theory reproduces the well-known properties of a sinusoidal grating. The direction of the scattered radiation is given by the grating equation $n_x - n_x^0 = \pm p/k$, and the efficiency of the grating increases with both the amplitude of the sinusoidal modulation and the reflectivity of the surface.

III. THE SCATTERING OF X RAYS FROM A MULTILAYER STRUCTURE

The extention of the theory of the scattering of x rays from a single nonideal interface to the case of a multilayer structure having nonideal interfaces is significantly complicated due to the interaction of the interfaces. In general, the radiation field scattered by each nonideal interface is a superposition of many plane wave modes. An exact accounting of the multiple scattering of every mode within the multilayer structure is intractable. Instead, a simplified picture of the interaction of the interfaces is required.

Recognizing that the scattering from each single interface is weak, it is tempting to ignore the interaction of the interfaces altogether. This is the standard kinematic approximation, where the total scattered field is simply the sum of the fields scattered from the incident field by each separate interface. However, the kinematic approximation is inappropriate for multilayer structures of practical interest because the total scattered field can be very strong; this is in fact the goal in designing efficient multilayer x-ray optics. In particular, a multilayer mirror typically consists of alternating layers of two materials having a periodic bilayer thickness D. Neglecting refractive effects, the structure has a strong specular reflection when

$$m\pi = Dk_0 n_z^0, \tag{61}$$

where m is an integer corresponding to the order of the reflection. Equation (61) represents the resonance condition at which the fields reflected specularly from each single interface add coherently, resulting in a total scattered field that is comparable in strength to the incident field.

In view of the coherent interaction of the interfaces, the multiple scattering cannot be completely neglected. A useful discussion of the interaction of x rays within a multilayer structure has been given by Spiller and Rosenbluth.[58] They point out that the nonspecular field within a multilayer is always weak compared to the specular field, because the nonspecular scattering of the incident field from the different interfaces is necessarily incoherent. The domination of the specular field suggests an approximate description of the interaction of the interfaces, referred to henceforth as the "specular field approximation." In this approximation, the specular field within the multilayer structure is treated dynamically and the nonspecular field is treated kinematically. Specifically, the specular field in each layer is determined from a complete dynamical treatment of the specular scattering within the system of interfaces, including all multiple scattering and extinction. In calculating the specular field, the nonspecular scattering is considered to remove energy from the specular field, but otherwise is neglected. In particular, no energy is coupled from the nonspecular field back into the specular field. The nonspecular field is then calculated using a kinematic treatment of the scattering of the specular field by the multilayer structure: The total field scattered into nonspecular directions is estimated as the sum of the nonspecular scattering from each interface.

A. Calculation of the scattered field

Let the multilayer structure be composed of a stack of N layers of dielectric media ϵ_i, as shown in Fig. 3, surrounded on both sides by vacuum. A plane wave of unit amplitude $\hat{e}^0 \exp(ik_0\hat{n}_0 \cdot \mathbf{x})$ is incident (at an angle θ) on the top of the stack. The propagation vector has components $n_x^0 = 0$, $n_y^0 = \sin\theta$, and $n_z^0 = \cos\theta$ and the polarization $\hat{e}$ is chosen to be either S or P type.

We begin by determining the specular field within the multilayer structure. The basic assumption of the specular field approximation is that the nonspecular field is weak compared to the specular field (including the incident field), and hence multiple scattering of the nonspecular field is neglected. The specular field in the ith layer away from either interface region is written as

$$E_i(\mathbf{x}) = e^{ik_0 n_y^0 y}(E_i^- \hat{e}^- e^{-ik_i n_z^i z} + E_i^+ \hat{e}^+ e^{ik_i n_z^i z}), \qquad (62)$$

where $k_i = |\epsilon_i^{1/2}|k_0$, and n_z^i is a complex quantity for an absorbing medium given by

$$n_z^i = \frac{1}{|k_i|}\sqrt{k_i^2 - k_0^2 n_y^{0^2}}. \qquad (63)$$

The polarization $\hat{e}^{\pm}$ in (62) corresponds to S or P type in accordance with the polarization of the incident field. The amplitudes E_i^- and E_i^+ of the specular field in each layer, as well as the amplitudes E^r and E^t of the reflected and transmitted fields above and below the stack, can be directly calculated using well-known recursive[8,29] or matrix[30,41] methods as discussed by Peterson, Knight, and Pen.[59] The application of these methods requires values for the amplitudes of specular reflection r_{ij} and transmission t_{ij} at each interface between adjacent layers i and j. The values are modified to account for the nonideal interfaces and are given to first order by

$$r_{ij} = r_{ij}^0 \tilde{w}_{ij}(-2k_0 n_z^0), \quad t_{ij} = t_{ij}^0. \qquad (64)$$

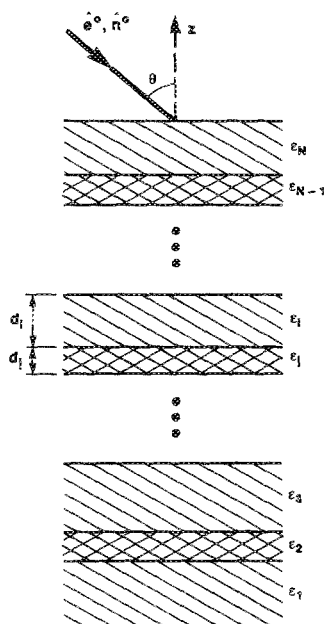Here r_{ij}^0 and t_{ij}^0 are the Fresnel amplitudes corresponding to the reflection and transmission from an ideal interface. As discussed in Sec. II E 2, the function $w_{ij}(z)$ characterizes the average gradient of the dielectric function across the interface, and $\tilde{w}_{ij}(s_z)$ is its Fourier transform. The specular reflectance and transmittance of the multilayer stack are then given by $|E^r|^2$ and $|E^t|^2$, respectively.

Once the specular field in each layer is determined, the nonspecular scattering is calculated kinematically; that is, the total nonspecular field is approximated as the sum of the fields scattered from each interface.

As an example, consider the reflected field scattered from the multilayer stack into the nonspecular direction $\hat{m}$ with polarization $\hat{a}$ where θ' is the angle between $\hat{m}$ and the normal to the stack and, for convenience, it is chosen that $m_x = 0$, $m_y = \sin\theta'$, and $m_z = \cos\theta'$. Then, in the ith layer the propagation direction of this mode is altered by refraction to have the value $\hat{m}^i$, where $m_x^i = 0$, $m_y^i = m_y$, and $m_z^i = (1/|k_i|)(k_i^2 - k_0^2\sin^2\theta')^{1/2}$.

There are two contributions to the nonspecular field from each interface, corresponding to the scattering from the interface of the specular fields incident on either side. In particular, consider the scattering from the interface between adjacent layers i and j. The specular fields incident on the interface from above and below are, correspondingly,

$$\mathbf{E}_1^{inc}(\mathbf{x}) = E_i^- \hat{e}^- e^{ik_0 n_y^0 y} e^{-ik_i n_z^i z}$$

and

$$\mathbf{E}_2^{inc}(\mathbf{x}) = E_j^+ \hat{e}^+ e^{ik_0 n_y^0 y} e^{ik_j n_z^j z}, \qquad (65)$$

where E_i^- and E_j^+ are determined using the matrix method as described above. Each of these specular fields scatters from the nonideal interface, producing a nonspecular field that propagates towards the top of the multilayer stack. The incident field $\mathbf{E}_1^{inc}$ scatters into the mode $\hat{m}^i$ with an amplitude r_{ij} given to first order by (21),

$$r_{ij}(\hat{m}^i,\hat{a};\hat{n}^i,\hat{e}^-) = E_i^- \frac{\Delta_{ij}k_i^2}{8\pi^2\epsilon_i}$$

$$\times (\hat{a}^* \cdot \hat{e}^-)\frac{\tilde{g}_{ij}[\,\mathrm{Re}(k_i\hat{m}^i - k_i\hat{n}^i)\,]}{m_z^i(m_z^i - n_z^i)}, \qquad (66)$$

where $g_{ij}(\mathbf{x})$ represents the ijth interface. Similarly, the incident field $\mathbf{E}_2^{inc}$ scatters into the mode $\hat{m}^i$ with an amplitude t_{ji} given by (31):

$$t_{ji}(\hat{m}^i,\hat{a};\hat{n}^i,\hat{e}^+) = -E_j^+ \frac{\Delta_{ji}k_j^3}{8\pi^2\epsilon_j}$$

$$\times (\hat{a}^* \cdot \hat{e}^+)\frac{\tilde{g}_{ji}[\,\mathrm{Re}(k_i\hat{m}^i - k_j\hat{n}^j)\,]}{m_z^i(k_i m_z^i - k_j n_z^j)}, \qquad (67)$$

where $g_{ji}(x,y,z) = g_{ij}(x,y,-z)$.

These two contributions to the nonspecular field propagate from the ith to the Nth layer accumulating a phase shift. The contribution to the phase shift from the pth layer is ϕ'_p given by

$$\phi'_p = k_0 d_p \sqrt{\epsilon_p - \sin^2\theta'}. \qquad (68)$$

FIG. 3. Configuration of the multilayer stack.

499   J. Appl. Phys., Vol. 65, No. 2, 15 January 1989

D. G. Stearns   499

The amplitude $R(\hat{m},\hat{a};\hat{n}^0,\hat{e}^0)$ of the total nonspecular field above the multilayer stack is the sum of the contributions from each interface.

$$R(\hat{m},\hat{a};\hat{n}^0,\hat{e}^0) = \sum_{\text{interfaces}} \left[\left(\prod_{p=i}^{N} e^{i\phi'_p} \right) \right.$$
$$\left. \times \left[r_{ij}(\hat{m}^i,\hat{a};\hat{n}^i,\hat{e}^-) + t_{ji}(\hat{m}^i,\hat{a},\hat{n}^i,\hat{e}^+) \right] \right].$$
(69)

Finally, the differential power scattered per unit solid angle is given by Eq. (24):

$$\frac{dP^r}{d\Omega}(\hat{m},\hat{a};\hat{n}^0,\hat{e}^0) = \frac{4\pi^2 m_z}{k_0^2 \tilde{g}(0)} |R(\hat{m},\hat{a};\hat{n}^0,\hat{e}^0)|^2.$$
(70)

B. Application: The reflectance and transmittance of x-ray beamsplitters

X-ray multilayer optics are finding increasing application in many areas of x-ray physics. As an example, there has recently been a successful demonstration of an efficient soft x-ray beamsplitter[60] which, as in the visible analog, divides an incident x-ray beam into approximately equal specularly reflected and transmitted components. The performance of multilayer x-ray optics is invariably degraded due to diffusion and mixing at the interfaces, as well as roughness of the layers replicated from the substrate or induced by processes such as polycrystalline growth. The nonideal interfaces not only modify the specular scattering, but can also scatter x rays into nonspecular directions. The nonspecular scattering is usually ignored, although it can be problematic in imaging applications and producing undesirable halos and background noise in the image field.

To investigate the effect of nonideal interfaces on the performance of multilayer x-ray optics, we calculate the specular scattering from two multilayer structures designed for use as x-ray beamsplitters. The specular reflectance and transmittance of the b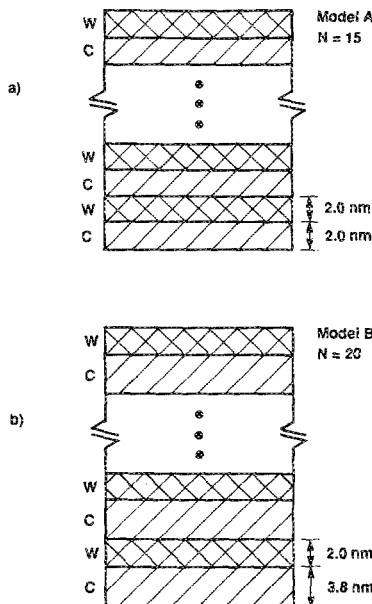eamsplitters is compared for a variety of different interface structures. Nonspecular scattering, which depends on the detailed frequency spectrum of the roughness of the interfaces, is not considered. All of the calculations presented here were performed on a VAX 11/780 computer using optical constants tabulated by Henke et al.[61]

The structures of the two beamsplitters, identified as models A and B, are shown in Figs. 4(a) and 4(b), respectively. The model A beamsplitter is composed of fifteen alternating layers of tungsten and carbon, each 2.0 nm thick. This beamsplitter is designed to operate at an x-ray wavelength of 1.0 nm and at an incident angle (measured from the normal to the surface) of 82.5°. The model B beamsplitter is composed of 20 bilayers of tungsten and carbon having thicknesses of 2.0 and 3.8 nm, respectively. It is designed to operate at a wavelength of 8.0 nm and an incident angle of 45°. These structures are assumed to be free standing for simplicity. In practice, the multilayers are usually supported by a membrane several tens of nanometers thick of a material of low absorption such as silicon nitride.

The calculated performance of the two beamsplitters when the interfaces are ideal is shown in Fig. 5. The reflectance, transmittance, and absorbance are plotted as a function of the angle of incidence of the x rays, which are assumed to be unpolarized. The reflectance of the model A beamsplitter, shown as the solid line in Fig. 5(a), exhibits a peak at 82.55° with a maximum value of 0.27 and a full width at half maximum (FWHM) of 0.50°. The transmittance (dashed line) and the absorbance (dotted line) are both observed to decrease in the vicinity of the peak in reflectance. The reflectance of the model B beamsplitter, shown in Fig. 5(b), peaks at 44.80° with a maximum value of 0.06 and a

FIG. 4. Ideal models of the structure of two x-ray beamsplitters composed of alternating layers of tungsten and carbon. (a) model A; (b) model B.
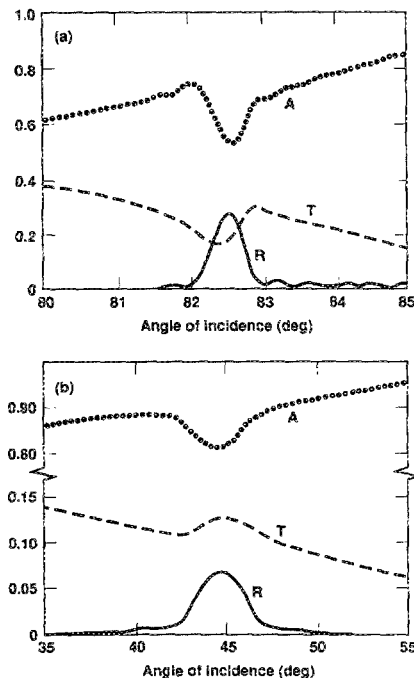

FIG. 5. Calculated reflectance (solid curve), transmittance (dashed curve), and absorbance (dotted curve) of the ideal beamsplitters as a function of the incident angle (measured from the normal) of the x-ray beam. The incident beam is unpolarized. (a) Model A beamsplitter, $\lambda = 1$ nm, (b) model B beamsplitter, $\lambda = 8$ nm.

FWHM of 2.65°. In this case the transmittance is enhanced in the vicinity of the reflectance peak, while the absorbance exhibits a decrease.

These two examples illustrate the variable behavior of the specular transmittance near the peak in reflectance for an x-ray beamsplitter. The transmittance can be either enhanced or attenuated depending on the design of the multilayer structure. The behavior of the transmittance for a particular multilayer is determined by the competition between two effects. The increase in specular reflection near the resonance condition (61) removes energy from the incident beam at the expense of the specular transmission. Hence a strong reflectance results in a decreased transmittance, as in the case of the model A beamsplitter. However, absorption of the incident beam is significant in x-ray multilayer optics, as shown in Fig. 5. The absorbance generally decreases near the resonance condition because the electric field consists of a standing wave[62] with the nodes positioned at the layers of the high-Z material (tungsten in the examples above). As a result, the highest intensity of the field is located in the regions of lowest absorption of the multilayer. The reduced absorbance at the resonance condition can enhance the transmittance if the reflectance is low, as in the case of the model B beamsplitter. The energy balance between the absorbance, reflectance, and transmittance of a beamsplitter is directly controlled by the choice of materials and structural parameters such as the thickness and the number of bilayers.

In practice, it is difficult to fabricate multilayer structures having interfaces that are ideal on the scale of an x-ray

wavelength. Figure 6 shows a high-resolution transmission electron microscope (HTEM) image of a cross section of an x-ray beamsplitter. The structure is composed of alternating layers of molybdenum and silicon of thicknesses 4.5 and 6.5 nm, respectively, deposited by magnetron sputtering onto a substrate consisting of a polished single-crystal silicon wafer coated with a 45-nm-thick layer of silicon nitride. The silicon wafer substrate is subsequently etched to leave the multilayers supported on a thin silicon nitride membrane. The HTEM image shows that the molybdenum layers are polycrystalline and the silicon layers are amorphous. The interfaces exhibit a combination of rough and diffuse structure. The interface roughness originates partly from replication of the roughness of the substrate, and additional roughness is induced by the crystal growth within the molybdenum layers. The diffuseness is most likely the result of mixing of molybdenum and silicon during deposition. Nonideal interfaces, particularly roughness replicated from the substrate, can be a very severe problem in the fabrication of multilayer beamsplitters.

The HTEM image illustrates the potential impact of nonideal interfaces on the structure of realistic multilayer x-ray optics. An example of the effect of nonideal interfaces on the performance of the model A beamsplitter is shown in Fig. 7. All of the interfaces are modified equivalently and are
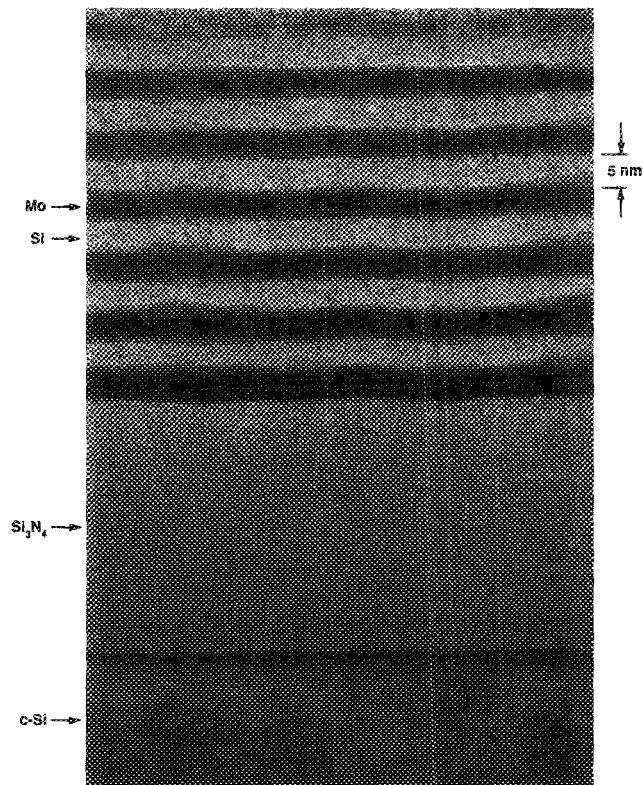

FIG. 6. High-resolution transmission electron microscope image of an x-ray beamsplitter designed for normal incidence operation at $\lambda = 20$ nm. The dark and light layers are molybdenum and silicon, respectively.
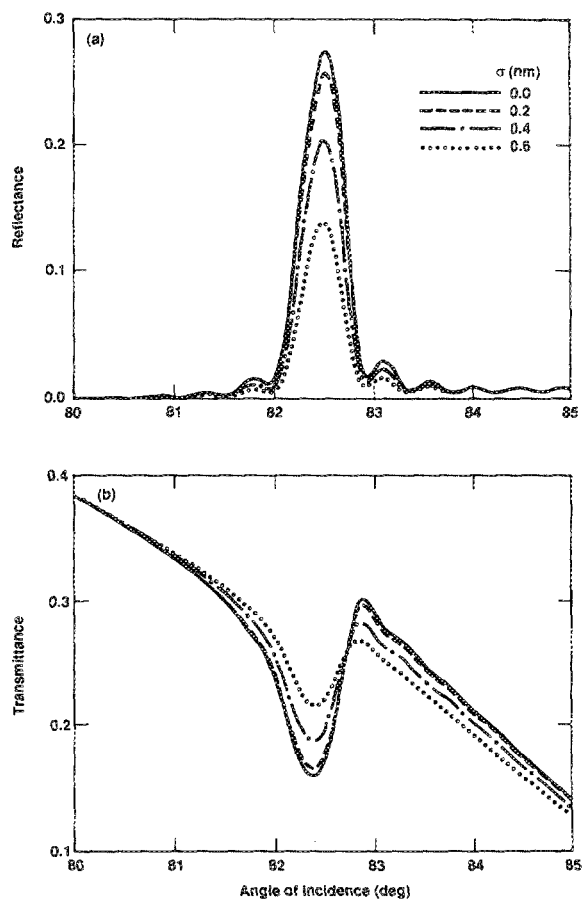

FIG. 7. Calculated performance of the model A beamsplitter with nonideal interfaces (error function profiles) as a function of the angle of incidence at $\lambda = 1$ nm. The curves correspond to interface widths that range from 0 to 0.6 nm. (a) Reflectance; (b) transmittance.

described by an error function profile of width σ. The reflectance [Fig. 7(a)] and transmittance [Fig. 7(b)] are shown for four values of σ varying between 0 and 0.6 nm. For larger values of σ the interfaces extend into the center of the layers, so that it would be necessary to represent the composition of the layers as a mixture of tungsten and carbon. It is apparent that the reflectance decreases with increasing σ, by as much as 50% at $\sigma = 0.6$ nm. In the vicinity of the reflectance peak the transmittance is observed to increase as σ increases, indicating a redistribution of energy from the reflected to the transmitted field.

A useful method of displaying the effect of nonideal interfaces is to plot the relative change in the reflectance $[R(\sigma) - R(\sigma = 0)]/R(\sigma = 0)$ as a function of the width σ of the interfaces. The change in reflectance for the model A beamsplitter at an incident angle of 82.55° (the peak position when the interfaces are ideal) is compared in Fig. 8(a) for the four different interface profiles listed in Table I. All four profiles cause the reflectance to decrease monotonically with increasing σ. It is also evident that for a particular interface width the change in reflectance is relatively insensitive to the choice of profile. It is found that the exponential profile causes slightly less attenuation of the reflectance than the linear, sinusoidal, and error function profiles. The relative change in transmittance of the model A beamsplitter at an incident angle of 82.40° is plotted in Fig. 8(b). The transmittance is observed to increase with increasing σ for all interface profiles. As in the case of the reflectance, the change in transmittance is approximately equivalent for all of the interface profiles.

For comparison, the relative change in reflectance (at

44.80°) and transmittance (at 45.40°) of the model B beamsplitter is plotted in Fig. 9 for the four different interface profiles. As before, the reflectance always decreases as the interface width increases. It is seen in Fig. 9(b), however, that the transmittance of the type B beamsplitter also decreases with increasing σ. In this case, the dominant effect of the nonideal interfaces is to increase the absorbance at the expense of both the reflectance and transmittance.

Close inspection of the curves in Fig. 7 shows that the relative change in the reflectance and transmittance of the model A beamsplitter varies with the angle of incidence, implying that the shape of the curves change with σ. This is shown explicitly in Fig. 10, where the change in reflectance and transmittance as a function of σ (assuming an error function profile) is plotted for three different angles of incidence. Referring to Fig. 10(a), it is seen that the peak of the reflectance curve at 82.55° decreases more slowly with σ than the reflectance on either side of the peak. This indicates that the peak narrows with increasing interface width. Such behavior can be understood physically by noting that as the reflectance of each interface decreases, the contribution to the reflected field from the interfaces at the bottom of the stack with respect to the top interfaces increases. The narrowest possible peak (highest resolution) is achieved when all of the interfaces contribute equally to the reflected field. Another feature observed in Fig. 10(a) is that reflectance on the high-angle side of the peak decreases more rapidly than the reflectance on the low-angle side, indicating that the peak shifts slightly with increasing σ, from a value of 82.55° at $\sigma = 0$ nm to 82.50° at $\sigma = 0.6$ nm. The complicated effect of nonideal interfaces on the transmittance at different angles of incidence is presented in Fig. 10(b). It is seen that the change in transmittance manifests a different sign depending on the incident angle. The increase in transmittance at angles less than 82.80° can be attributed to the corresponding decrease in reflectance.
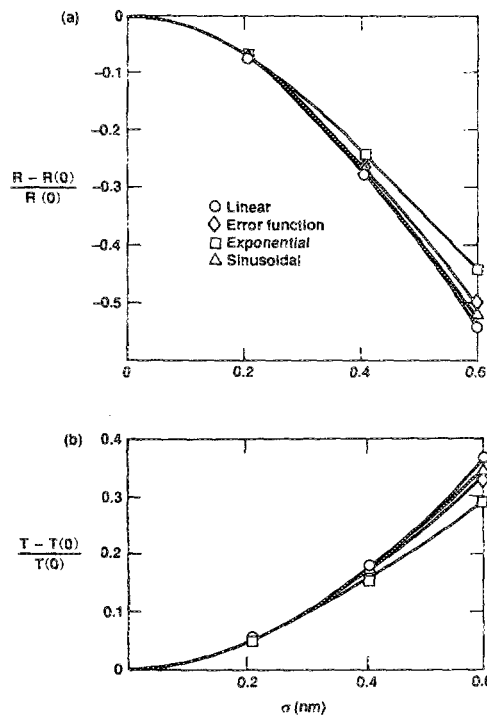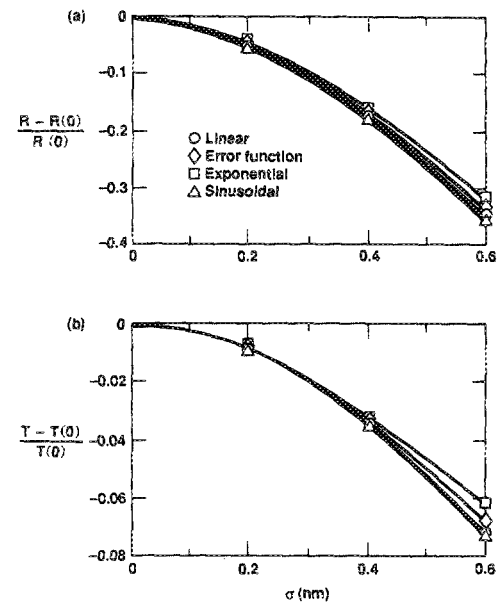

FIG. 8. The relative change of reflectance and transmittance of the model A beamsplitter as a function of interface width for different interface profiles at $\lambda = 1$ nm. (a) Reflectance, $\theta = 82.55°$; (b) transmittance, $\theta = 82.40°$.

FIG. 9. The relative change of reflectance and transmittance of the model B beamsplitter as a function of interface width for different interface profiles at $\lambda = 8$ nm. (a) Reflectance, $\theta = 44.80°$; (b) transmittance, $\theta = 45.40°$.
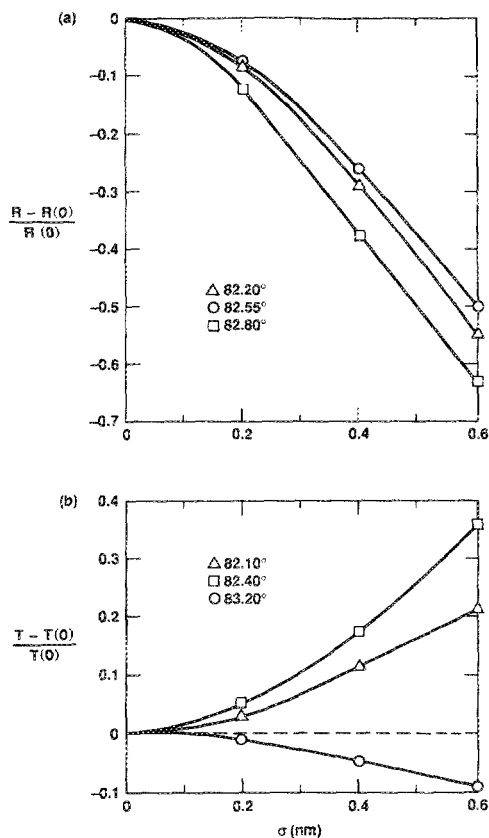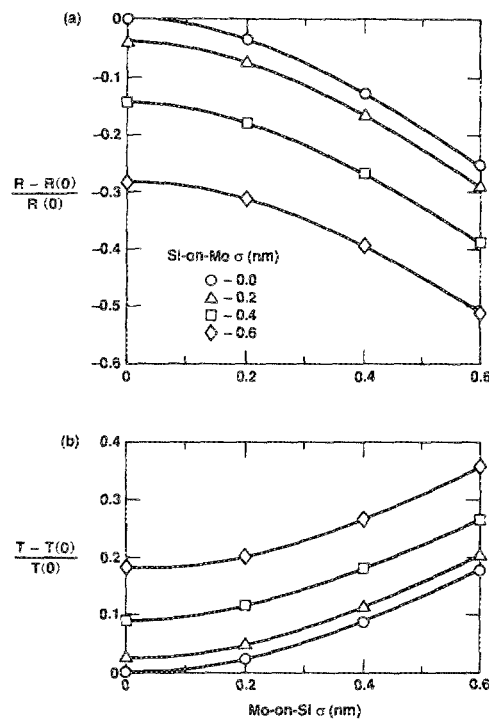
FIG. 11. The relative change of reflectance and transmittance of the model A beamsplitter at $\lambda = 1$ nm as a function of the width of the tungsten-on-carbon interface for different values of the width of the carbon-on-tungsten interface. (a) Reflectance, $\theta = 82.55°$; (b) transmittance, $\theta = 82.40°$.

FIG. 10. The relative change of reflectance and transmittance of the model A beamsplitter as a function of interface width (error function profiles) at $\lambda = 1$ nm and at different angles of incidence. (a) Reflectance; (b) transmittance.

Thus far all of the interfaces of the beamsplitter have been assumed to be identical. In practice, the nature of an interface can vary significantly according to its deposition history as well as its orientation within the layer stack. A important example is the asymmetry observed in the interface widths of sputtered multilayer structures.[60] It is found that the interfaces created by sputtering the high-Z material onto a low-Z material are generally wider than the opposite case. This is attributed to an increased mixing at the interface driven by the greater kinetic energy of the heavier atoms. The relative change in the reflectance and transmittance of a model A beamsplitter having asymmetric nonideal interfaces is shown in Fig. 11. The change is plotted as a function of the width of the tungsten-on-carbon interface, for four different widths of the carbon-on-tungsten interface, as each is allowed to vary between 0 and 0.6 nm. All of the interfaces are described by an error function profile. It is seen that an increase in the width of either type of interface causes a decrease in reflectance and a corresponding increase in transmittance. Furthermore, the relative change in performance induced by one type of interface is independent of the width of the other type of interface.

It has also been observed that the width of the interfaces in a multilayer structure can vary according to position within the stack.[63,64] The most common situation is that the width of the interfaces either monotonically increases or decreases on going from the bottom to the top of the stack. The former case occurs if roughness accumulates during depo-

sition, so that each successive layer replicates the roughness of previous layers and contributes additional roughness. The latter case occurs if the deposition of each successive layer anneals roughness that was originally introduced by the substrate. The specific behavior of a multilayer system depends on the materials and the parameters of the deposition process. The modification of the performance of the model A beamsplitter when the interface widths are made to vary linearly with position within the stack is shown in Fig. 12. The dashed curve corresponds to a structure in which the interface width increases linearly from 0 nm at the top of the stack to 0.6 nm at the bottom. The dotted line represents the complementary case in which σ varies from 0.6 nm at the top of the stack to 0 nm at the bottom. For comparison, the solid line represents the performance of the beamsplitter with ideal interfaces. In both cases the reflectance, shown in Fig. 12(a), is reduced by the introduction of nonideal interfaces. The case in which the widest interfaces are on top exhibits the largest decrease in reflectance because the top interfaces contribute the most to the reflected field. In contrast, in Fig. 12(b) it is seen that the transmittance of the two nonideal structures is nearly identical. This indicates that the transmittance averages over the variation in interface widths, and is not particularly sensitive to the orientation of the interfaces within the stack. Hence, in an effort to optimize performance, it is always desirable to choose materials and deposition parameters that produce multilayer structures in which the interface width is minimized at the top of the stack.

In conclusion, it has been found that the performance of a multilayer x-ray beamsplitter is significantly affected by
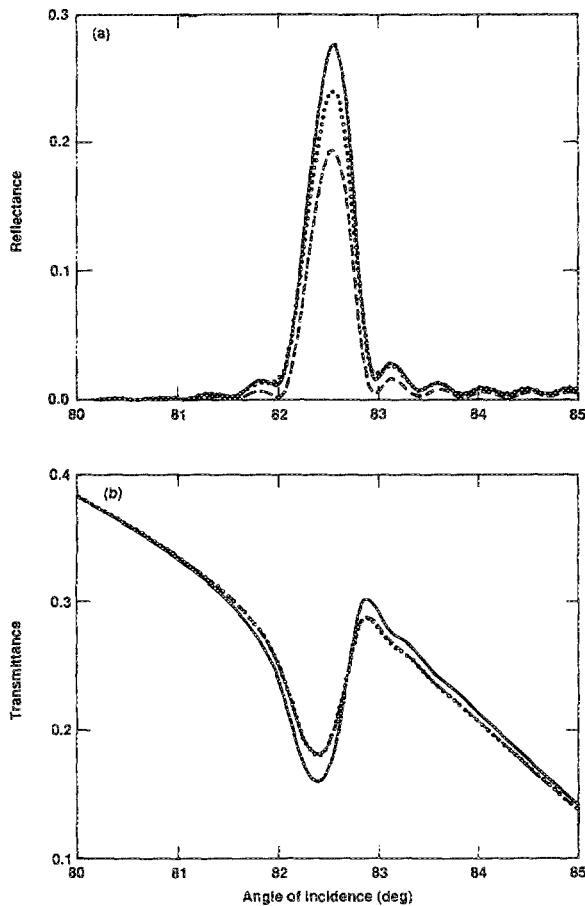
FIG. 12. Calculated performance of the model A beamsplitter at $\lambda = 1$ nm as a function of incident angle for the case of ideal interfaces (solid curve), and when the width of the interfaces increases (dashed curve) and decreases (dotted curve) from the top to the bottom of the multilayer stack. (a) Reflectance; (b) transmittance.

the structure of the interfaces. In general, the reflectance is observed to decrease as the width of the interfaces increases; the transmittance can either decrease or increase depending on the design of the beamsplitter. It has been seen that the reflectance and transmittance are sensitive to structural details such as the variation of interfaces widths within the multilayer stack, and yet are relatively insensitive to the precise shape of the interface profiles.

This example demonstrates that the existence of nonideal interfaces must be taken into account to accurately design and model realistic x-ray multilayer optics. Consequently, it is important to thoroughly characterize the interface structure of the standard multilayer systems, such as carbon and tungsten, acquiring information about interface widths, profiles, and the frequency spectrum of the roughness. The scattering theory developed in this work, in conjunction with such detailed structural information, provides a general and powerful foundation for understanding the x-ray scattering from nonideal multilayer structures.

ACKNOWLEDGMENTS

APPENDIX A: THE DIELECTRIC FUNCTION REPRESENTATION

The interaction of electromagnetic radiation and matter on a macroscopic scale is described by the dielectric function $\epsilon(x,\omega)$, which relates the polarization $P(x,\omega)$ of a medium to the electric field $E(x,\omega)$ through

$$\epsilon(x,\omega) = 1 + \frac{4\pi|P(x,\omega)|}{|E(x,\omega)|}. \tag{A1}$$

From a quantum-mechanical point of view, the dielectric function represents the response of a dielectric medium to the radiation field through all the possible virtual and real transitions of the solid-state system. Besides atomiclike excitations, the dielectric function also includes contributions from the bulk collective excitations such as plasmons, as well as surface excitations such as surface plasmons that are associated with the interfaces. In principle, the dielectric function is sensitive to solid-state effects such as chemical bonding and collective excitations. Fortunately, in the case of x rays having wavelengths less than ~ 10 nm, these effects can be neglected. This is because the energies of these excitations are much less than the x-ray energy, so that the valence electrons respond to the field as free electrons. Consequently, at x-ray wavelengths the dielectric function is isotropic and depends only on the atomic composition and density of the matter, not on the detailed structure of the solid-state system.

It is useful to relate the dielectric constant of a material to its atomic composition. The response of an atom to an applied field of amplitude E is described by the atomic dipole moment p_a,

$$p_a = p_e(f_1 + if_2), \tag{A2}$$

where $f_1 + if_2$ is the complex atomic scattering factor and p_e is the dipole moment of a free electron, given by

$$p_e = -(r_e\lambda^2/4\pi^2)E. \tag{A3}$$

Here r_e is the classical electron radius and λ is the x-ray wavelength in vacuum.

The major assumption of the dielectric function representation is that the spatial variation of the applied field is negligible over a small volume V (which is, however, large compared to an atomic volume), so that all of the atomic dipole moments within V oscillate in phase. Then the polarization P per unit volume is simply the sum of the atomic moments,

$$P = (1/V)\Sigma p_a. \tag{A4}$$

Using Eq. (A1), the dielectric function is related to the atomic scattering factors through

$$\epsilon(x,\omega) = 1 - \frac{r_e\lambda^2}{\pi}\sum_j \frac{N_j(x)\rho(x)A}{w(x)}[f_1^j(\omega) + if_2^j(\omega)], \tag{A5}$$

where ρ is the density of the medium, A is Avogadro's number, w is the molecular weight of the medium, N_j is the number of atoms of type j in a molecule, and the sum is over the different types of atoms. A comprehensive tabulation of the atomic scattering factors can be found in Ref. 61.

The dielectric function representation is commonly used to describe the propagation of x rays in matter. It is important, however, to appreciate the limitations of this representation. By definition, the dielectric function contains an implicit spatial average over a microscopic volume that removes spatial variations of the polarization on the atomic scale.[65] Hence, $\epsilon(\mathbf{x})$ contains no information about the atomic structure of matter. Nonetheless, it is well known that x rays scatter from polarization fluctuations on the atomic scale, as in the Bragg scattering from crystal lattices. Specifically, an x ray of wavelength λ can scatter elastically from polarization fluctuations having spatial frequencies up to a value $4\pi c/\lambda$, corresponding to the maximum possible change of momentum of the x ray. This implies that the dielectric function representation is only valid at x-ray wavelengths that are larger than the spatial scale of the atomic structure. In view of this limitation, the scattering theory developed in this work is only strictly valid for wavelengths greater than ~ 1 nm. In practice, the theory can be applied to shorter wavelengths with caution, as long as there is no strong coherent scattering from the atomic structure. This should particularly be the case when the materials are amorphous.

APPENDIX B: SCATTERING IN THE FAR FIELD

In this Appendix an expression is derived for the reflected radiation in the far-field limit. Consider the radiation field at the position $\mathbf{x} = R\hat{n}$ in the limit that $R \to \infty$. A minor rearrangement of (20) yields

$$\hat{e}^* \cdot \mathbf{E}^r(R\hat{n}) = \int\int r(\hat{m},\hat{e};\hat{n}^0,\hat{e}^0)e^{ikR(\hat{n}\cdot\hat{m})}\, dm_x\, dm_y.$$
(B1)

Note that any evanescent mode $\hat{m}$ where $m_x^2 + m_y^2 > 1$ will not contribute to the field at $\mathbf{x} = R\hat{n}$ because m_z is imaginary. Hence the integrand vanishes everywhere outside of the unit circle in the $m_x - m_y$ plane, providing the boundary condition

$$e^{ikR(\hat{n}\cdot\hat{m})}\Big|_C^{R\to\infty} = 0,$$
(B2)

where C represents the unit circle. It is convenient to make a variable transformation to polar coordinates (θ,ϕ). Specifically, the points (m_x, m_y) inside the unit circle C are mapped onto the unit hemisphere. Without loss of generality, the polar axis is chosen to be in the direction $\hat{n}$. Then,

$$\hat{m}\cdot\hat{n} = \cos\theta.$$
(B3)

The differential area $dm_x\, dm_y$ is simply the projection of the infinitesimal area $d\Omega$ of the unit sphere onto the $m_x - m_y$ plane:

$$dm_x\, dm_y = m_z\, d\Omega = m_z \sin\theta\, d\theta\, d\phi.$$
(B4)

Then (B1) can be written

$$\hat{e}^* \cdot \mathbf{E}^r(R\hat{n}) = \int_0^{2\pi}\int_0^{\theta_C(\phi)} r[\hat{m}(\theta,\phi),\hat{e};\hat{n}^0(\theta,\phi),\hat{e}^0]$$

$$\times m_z(\theta,\phi)e^{ikR\cos\theta}\sin\theta\, d\theta\, d\phi.$$
(B5)

The upper limit on the integral over θ is the angle $\theta_C(\phi)$ at which the unit vector $\hat{m}$ lies in the $m_x - m_y$ plane, and is imposed by the boundary condition (B2).

The integral over θ is evaluated using repeated integration by parts to generate a series of terms in increasing powers of $(1/R)$. For example, the first integration by parts yields

$$\hat{e}^* \cdot \mathbf{E}^{sc}(R\hat{n}) = -\int_0^{2\pi}\left(r(\hat{m},\hat{e};\hat{n}^0,\hat{e}^0)m_z\frac{e^{ikR\cos\theta}}{ikR}\right)_{\theta=0}^{\theta=\theta_C(\phi)} d\phi$$

$$+\int_0^{2\pi}\int_0^{\theta_C(\phi)}\frac{\partial}{\partial(\cos\theta)}[r(\hat{m},\hat{e};\hat{n}^0,\hat{e}^0)m_z]$$

$$\times\frac{e^{ikR\cos\theta}}{ikR}d(\cos\theta)d\phi,$$
(B6)

Integrating the second term by parts once more shows that this term is proportional to $(1/R)^2$ and thus is negligible as $R\to\infty$. The first term vanishes at the upper limit $\theta = \theta_c$ due to the boundary condition (B2). At the lower limit $(\theta = 0)$ we note that $\hat{m} = \hat{n}$, and the first term is evaluated to yield

$$\hat{e}^* \cdot \mathbf{E}^r(R\hat{n}) = -(2\pi i n_z/k)r(\hat{n},\hat{e};\hat{n}^0,\hat{e}^0)(e^{ikR}/R).$$
(B7)

[1] T. W. Barbee, Jr., Opt. Eng. 25, 898 (1986).
[2] E. Spiller, Appl. Phys. Lett. 20, 365 (1972).
[3] E. Spiller, Appl. Opt. 15, 2333 (1976).
[4] R.-P. Haelbich and C. Kunz, Opt. Commun. 17, 287 (1976).
[5] A. V. Vinogradov and B. Y. Zeldovich, Opt. Spectrosc. 42, 404 (1977); Appl. Opt. 16, 89 (1977).
[6] R. -P. Haelbich, A. Segmuller, and E. Spiller, Appl. Phys. Lett. 34, 184 (1979).
[7] T. W. Barbee, Jr. and D. L. Keith, in Synthesis and Properties of Metastable Phases, edited by E. S. Machlin and T. J. Roland (AIME, New York, 1980), p. 93.
[8] J. H. Underwood and T. W. Barbee, Jr., Appl. Opt. 20, 3027 (1981).
[9] E. Spiller, A. Segmuller, J. Rife, and R. -P. Haelbich, Appl. Phys. Lett. 37, 1048 (1981).
[10] J. V. Gilfrich, D. J. Nagel, N. G. Loter, and T. W. Barbee, Jr., in Advances in X-ray Optics, edited by J. C. Russ, C. S. Barrett, P. K. Predecki, and D. E. Leyden (Plenum, New York, 1981), Vol 25, p. 355.
[11] P. Lee, Opt. Commun. 37, 159 (1981); Opt. Commun. 42, 195 (1982).
[12] A. E. Rosenbluth, Ph.D. thesis, University of Rochester, 1982.
[13] R. Day, J. Grosso, R. Bartlett, and T. Barbee, Nucl. Instrum. Methods 208, 245 (1983).
[14] T. W. Barbee, Jr., in X-ray Microscopy, edited by G. Schmahl and D. Rudolph (Springer, New York, 1984), p. 144.
[15] T. W. Barbee, Jr., S. Mrowka, and M. C. Hettrick, Appl. Opt. 24, 883 (1985).
[16] P. Lee, R. J. Bartlett, and D. R. Kania, Opt. Eng. 24, 197 (1985).
[17] I. V. Kozivnikov and A. V. Vinogradov, Phys. Scr. T17, 137 (1987).
[18] F. E. Fernandez, C. M. Falco, P. Dhez, A. Khandar-Shahabad, L. Nevot, B. Pardo, J. Corno, and B. Vidal, Appl. Phys. Lett. 51, 880 (1987).
[19] G. F. Marshall, Ed., Applications of Thin-Film Multilayered Structures to Figured X-ray Optics, Proc. SPIE (SPIE, Bellingham, WA, 1985), Vol. 563.
[20] N. M. Ceglio and P. Dhez, Eds., Multilayered Structures and Laboratory X-ray Laser Research, Proc. SPIE (SPIE, Bellingham, WA, 1986), Vol. 688.
[21] L. V. Knight and D. K. Bowen, Eds., X-ray Imaging II, Proc. SPIE (SPIE, Bellingham, WA, 1986), Vol 691.
[22] E-E. Koch and G. Schmahl, Eds., Soft X-ray Optics and Technology, Proc. SPIE (SPIE, Bellingham, WA, 1986), Vol. 733.
[23] J. H. Underwood, T. W. Barbee, Jr., and D. C. Keith, Proc. SPIE 184, 123 (1979).
[24] J. P. Henry, E. Spiller, and M. Weisskopf, Appl. Phys. Lett. 40, 25 (1982).

505   J. Appl. Phys., Vol. 65, No. 2, 15 January 1989

D. G. Stearns   505

[25] J. H. Underwood and T. W. Barbee, Jr., Nature **294**, 429 (1981).

[26] D. H. Bilderback, B. M. Lairson, T. W. Barbee, Jr., G. E. Ice, and C. J. Sparks, Nucl. Instrum. Methods **208**, 251 (1983).

[27] E. Ziegler, Y. Lepetre, I. K. Schuller, and E. Spiller, Appl. Phys. Lett. **48**, 1354 (1986).

[28] N. M. Ceglio, D. G. Stearns, A. M. Hawryluk, T. W. Barbee, K. Danzmann, M. Kuhne, P. Muller, B. Wende, M. B. Stearns, A. K. Petford-Long, and C-H. Chang, J. Phys. (Paris) **47**, C6-277 (1986).

[29] L. G. Parratt, Phys. Rev. **95**, 359 (1954).

[30] M. Born and E. Wolf, *Principles of Optics*, 3rd ed. (Pergamon, New York, 1965), p. 51.

[31] A. K. Petford-Long, M. B. Stearns, C-H. Chang, S. R. Nutt, D. G. Stearns, N. M. Ceglio, and A. M. Hawryluk, J. Appl. Phys. **61**, 1422 (1987).

[32] M. B. Stearns, C. H. Lee, C.-H. Chang, and A. K. Petford-Long, in *Metallic Multilayers and Epitaxy*, edited by S. Wolf and B. C. Gubser (AIME, Warrendale, PA, 1988), p. 55.

[33] J. B. Kortright and J. D. Denlinger, MRS Symp. Proc. **103**, 95 (1988).

[34] G. M. Lamble, S. M. Heald, D. E. Sayers, and E. Ziegler, MRS Symp. Proc. **103**, 101 (1988).

[35] For instance, H. Davies, Proc. IEE, Pt. III, **101**, 209 (1954).

[36] P. Beckmann and A. Spizzichino, *The Scattering of Electromagnetic Waves from Rough Surfaces* (Pergamon, New York, 1963).

[37] H. E. Bennett and J. O. Porteus, J. Opt. Soc. Am. **51**, 123 (1961).

[38] J. O. Porteus, J. Opt. Soc. Am. **53**, 1394 (1963).

[39] I. Ohlidal, K. Navratil, and F. Lukes, J. Opt. Soc. Am. **61**, 1630 (1971).

[40] A. K. Fung, Can. J. Phys. **48**, 127 (1970).

[41] J. M. Eastman, in *Physics of Thin Films, Advances in Research and Development*, edited by G. Hass and M. H. Francombe (Academic, New York, 1978), Vol. 10, p. 167.

[42] C. K. Carniglia, Opt. Eng. **18**, 104 (1979).

[43] J. M. Elson, App. Opt. **16**, 2872 (1979).

[44] P. Bousquet, F. Flory, and P. Roche, J. Opt. Soc. Am. **71**, 1115 (1981).

[45] P. Croce, Nouv. Rev. Opt. Appl. **3**, 249 (1972).

[46] P. Croce and L. Prod'homme, Nouv. Rev. Opt. **7**, 121 (1976).

[47] W. Ehrlenberg, J. Opt. Soc. Am. **39**, 746 (1949).

[48] L. Nevot and P. Croce, Rev. Phys. Appl. **15**, 761 (1980).

[49] P. Croce, J. Opt. **14**, 1 (1983); P. Croce, J. Opt. **14**, 4 (1983).

[50] B. Vidal and P. Vincent, Appl. Opt. **23**, 1794 (1984).

[51] A. Roger, Opt. Acta **30**, 575 (1983).

[52] S. K. Sinha, E. B. Sirota, S. Garoff, and H. B. Stanley, Phys. Rev. B **38**, 2297 (1988).

[53] J. D. Jackson, *Classical Electrodynamics*, 2nd ed. (Wiley, New York, 1975), p. 420.

[54] A. L. Fetter and J. D. Walecka, *Theoretical Mechanics of Particles and Continua* (McGraw-Hill, New York, 1980), p. 316.

[55] Recall that the lateral extent of the interface is considered to be infinite. It is necessary that the limits $X \to \infty$, $Y \to \infty$, and $R \to \infty$ be taken such that $R \gg X$ and Y. This assures that the interface scatters as a point source in the far field.

[56] R. Giacconi, W. P. Reidy, G. S. Vaiana, L. P. Van Speybroeck, and T. F. Zehnpfennig, Space Sci. Rev. **9**, 3 (1969).

[57] J. M. Eastman and P. W. Baumeister, Opt. Commun. **12**, 418 (1974).

[58] E. Spiller and A. E. Rosenbluth, Proc. SPIE **563**, 221 (1985).

[59] B. G. Peterson, L. V. Knight, and H. K. Pew, Proc. SPIE **563**, 328 (1985).

[60] D. G. Stearns, N. M. Ceglio, A. M. Hawryluk, M. B. Stearns, A. K. Petford-Long, C-H. Chang, K. Danzmann, M. Kuhne, P. Muller, and B. Wende, Proc. SPIE **563**, 91 (1985).

[61] B. L. Henke, P. Lee, T. J. Tanaka, R. L. Shimabukuro, and B. K. Fujikawa, At. Data Nucl. Data Tables **27**, 1 (1982).

[62] A nice discussion is given in Ref. 3.

[63] E. Spiller, Proc. SPIE **563**, 367 (1985).

[64] J. R. McNeil, L. J. Wei, G. A. Al-Jumaily, S. Shakir, and J. K. McIver, App. Opt. **24**, 480 (1985).

[65] J. D. Jackson, *Classical Electrodynamics*, 2nd ed. (Wiley, New York, 1975), p. 226.